

We are IntechOpen, the world's leading publisher of Open Access books Built by scientists, for scientists

5,800

Open access books available

142,000

International authors and editors

180M

Downloads

Our authors are among the

154

Countries delivered to

TOP 1%

most cited scientists

12.2%

Contributors from top 500 universities



WEB OF SCIENCE™

Selection of our books indexed in the Book Citation Index
in Web of Science™ Core Collection (BKCI)

Interested in publishing with us?
Contact book.department@intechopen.com

Numbers displayed above are based on latest data collected.
For more information visit www.intechopen.com



Chapter

Design, Analysis and Testing of Piezoelectric Tool Actuator for Elliptical Vibration Cutting

Jinguo Han, Mingming Lu and Jieqiong Lin

Abstract

In the field of ultraprecision machining, the structured surfaces with various micro/nano characteristics may have different advanced functions, such as wettability modifications, tribological control and hybrid micro-optics. However, the machining of micro/nano structured surfaces is becoming a challenge for present cutting method. Especially for the difficult-to-cut materials, it is impossible to manufacture complex micro/nano features by using traditional cutting methods. The complex features require a cutting tool no longer confined to the traditional motion guide. The cutting tool should have more quick response velocity and flexible modulated ability. This chapter aims to make an introduction for piezoelectric tool actuator used in elliptical vibration cutting, which can be offering tertiary cutting operations with quick response and flexible modulated ability. The content covers the working principle of piezoelectric tool actuator, compliant mechanism design, static modeling, kinematic and dynamic modeling, structure optimization and offline testing.

Keywords: piezoelectric actuator, elliptical vibration cutting, compliant mechanism, ultraprecision machining, structured surface

1. Introduction

With the rapid growth of science and technology, precision components are increasingly in demand in various fields such as aerospace, biomedical engineering, optics, surface engineering and energy. These components not only require tight tolerances and high-quality surface finishes but also require the use of difficult-to-cut materials like high-temperature alloys and hard-brittle materials owing to the physical, mechanical, optical and electronic properties [1]. It is because of the difficult-to-cut characteristics, the precision machining of these materials has always been a challenge. For traditional machining methods, there are always some disadvantages, such as high cutting temperature and cutting force, severe tool wear, low efficiency and poor surface quality. To improve the manufacturing quality, tool life and machining efficiency, let the machining cost down, elliptical vibration-assisted machining (EVAM) was proposed. In ultraprecision machining, especially the structured surface

with micro-nano features, it requires exceptionally fine and repeatable motions, which makes the piezoelectric actuator a popular candidate for EVAM.

In EVAM, the elliptical vibration cutting (EVC) is a typical method for turning. It has been validated that EVC can improve the machinability of difficult-to-cut materials [2–4]. Meanwhile, the lower cutting force, longer tool life and better machining quality were obtained. In EVC, the vibration of cutting tool or workpiece is usually motivated by external excitation. For elliptical vibration cutting, the locus of cutting tool or workpiece is an ellipse due to the deliberate modulation of vibration devices. According to the principle of vibration, vibration devices can be divided into two types: resonant vibration and non-resonant vibration. For resonant type EVC vibrator, usually consists of an ultrasonic generator, a transducer and an ultrasonic vibration horn. The working frequency is generally above 20 kHz. There are two design schemes for the structure configuration, i.e. patch and sandwich. For the patch type EVC vibrator, two sets of piezoelectric plates are attached to the outer wall of the resonant rod to achieve the same or different modes of resonance. What's more, the Langevin-type transducer is usually adopted in the sandwich-type EVC vibrator. The vibrator can be achieved by adding two or more sets of piezoelectric rings to the resonant rod or coupling two Langevin-type transducers. The ellipse locus of cutting tool can be obtained through the same or different modes coupling in different directions with the nearly same vibration frequency. The working frequency is the resonance frequency. Additionally, the fixed working frequency and vibration parameters, poor dynamic accuracy and open-loop control, heat generation problems are the limitation problems for the resonant vibrator.

For non-resonant type EVC vibrator, usually consists of piezoelectric actuators and a compliant mechanism with deliberate design. Compared with the resonant vibration, the non-resonant type EVC vibrator provides much higher flexibility due to the elastic deformation of compliant mechanism. The vibration parameters like amplitude and frequency are easy to be controlled. The micro-nano motion resulting from elastic deformation of flexure hinge can guarantee the modulation ability and accuracy, which makes it more suitable for the manufacturing of micro-nano structured surfaces.

Generally, compared with workpiece vibration, tool vibration is more popular due to the ease of implementation. In fact, the modulation capability of tools plays a very important role in manufacturing for different materials and structure features. However, the tool modulation capability mainly depends on the performance of the vibrator. Obviously, the non-resonant type EVC vibrator has more advantages than the resonant type EVC vibrator. Up to now, there are many different types of non-resonant EVC vibrators were developed for vibration machining. Therefore, this chapter mainly focuses on the non-resonant type EVC vibrator, aiming to review the working principle of piezoelectric tool actuator, compliant mechanism design, static modeling, kinematic and dynamic modeling, structure optimization and offline testing.

2. Introduction to the different types of EVC

EVC is a kind of vibration-assisted machining. Different from 1-dimensional vibration cutting and traditional cutting, the trajectory of cutting tool is an ellipse and it is located in a fixed plane (2-dimensional, 2D) or in space (3-dimensional, 3D) which is dependent on the vibration modulation of motion axis. The cutting process of different types of EVC is shown in **Figure 1**. It can be seen that for orthogonal EVC and oblique EVC, the tool trajectory is in a fixed plane despite the orientation of fixed

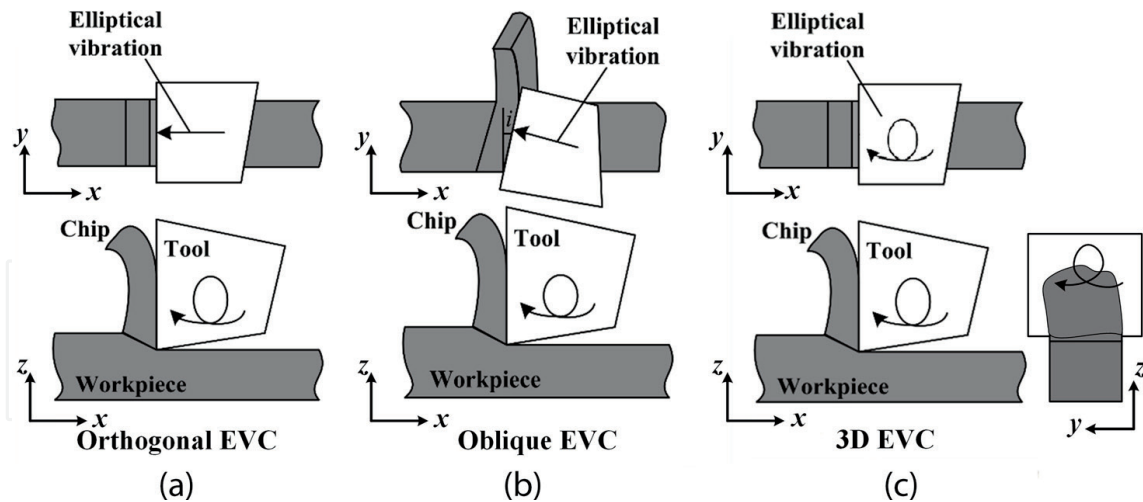


Figure 1.
 Schematic illustration of different types of EVC.

plane in oblique EVC is also dependent on the angle i . It only needs two motion axes to modulate the cutting tool to obtain the ellipse locus. However, for 3D EVC, the trajectory of cutting tool is in space or in an arbitrary plane of modulation range. Therefore, it needs at least three motion axes to obtain the ellipse locus.

3. Development of the non-resonant type EVC vibrator

3.1 2D type EVC vibrator

The EVC method is first proposed based on a 2D type EVC vibrator. Therefore, the research on 2D type EVC vibrator is relatively early and extensive. According to the principle of EVC, generally, there are two piezoelectric actuator configurations for the simplest: one is there existing an angle between two piezoelectric actuators, the other one is piezoelectric actuator parallel configuration. Shamoto and Moriwaki applied the vertical piezoelectric actuator configuration to achieve the EVC [5]. Cerniway [6] and Negishi [7] applied parallel piezoelectric actuator configuration to achieve the EVC. However, these non-resonant EVC vibrators have limited modulation ability and severe crosstalk. In recent years, the flexure-based non-resonant EVC vibrator has been developing rapidly. Here are some typical examples following below.

3.1.1 A hybrid flexure hinge EVC vibrator actuated by parallel piezoelectric actuator configuration

3.1.1.1 Orthogonal type

In this work, a hybrid flexure hinge EVC vibrator actuated by parallel piezoelectric actuators was proposed [8]. The mechanical structure of the vibrator is shown in **Figure 2(a)**. The coordinate system $O_{out}-xyz$ is fixed on the end-effector. The mechanical structure has mirror symmetry about the y -axis. Two piezoelectric actuators, which are placed in parallel from top to bottom and directly preloaded by two screws, are used to actuate the motion of the cutting tool. There are four motion guidance components in the mechanical structure, i.e. two double parallel four-bar

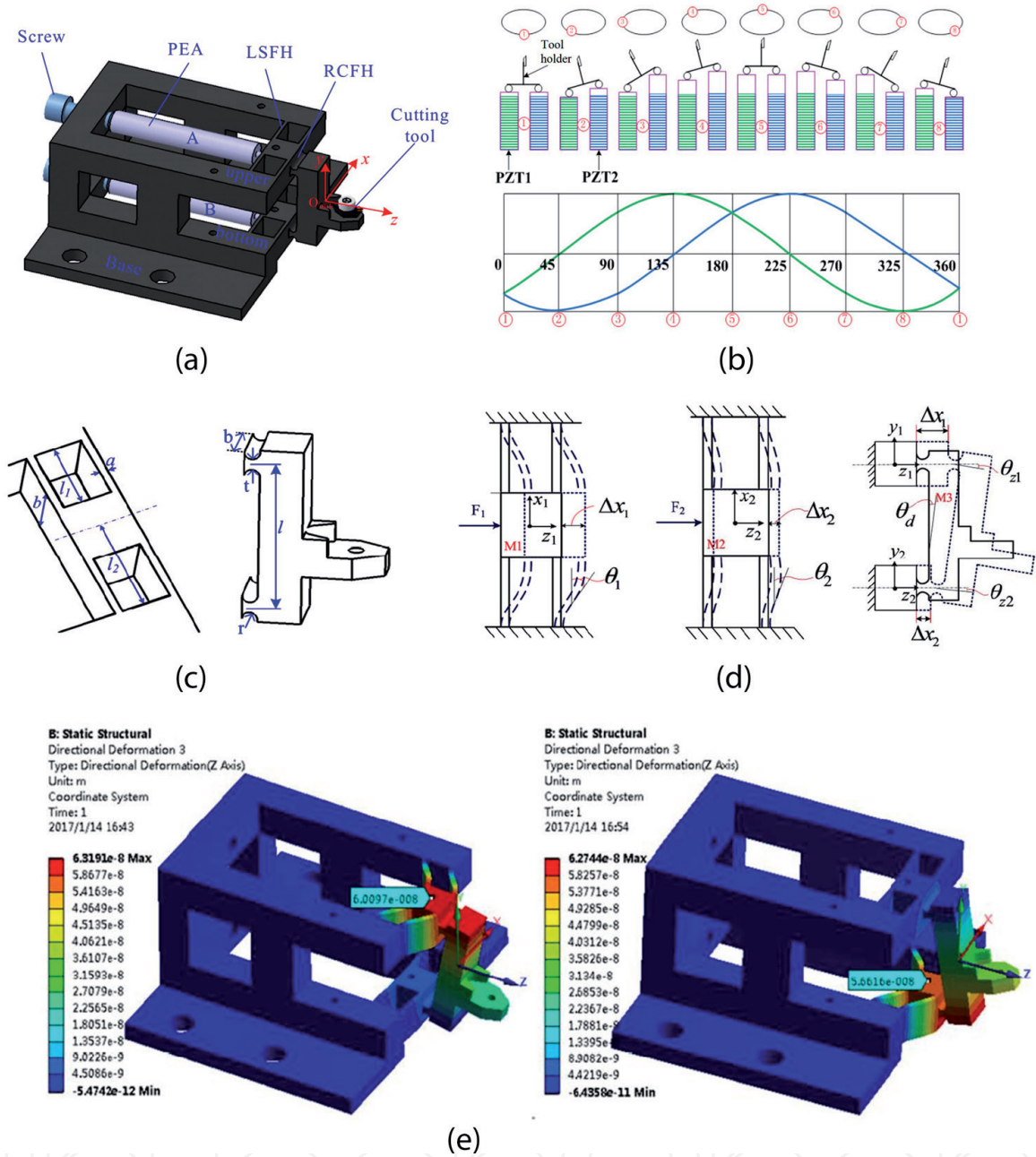


Figure 2. Illustration of the proposed hybrid flexure hinge EVC actuated by a parallel piezoelectric actuator. (a) Mechanical structure. (b) Working principle. (c) Two types of flexure hinge. (d) Deformation schematic of flexure-based mechanism. (e) FEM simulation [8].

linkage mechanisms and two right circular flexure hinges. The double parallel four-bar linkage mechanism is connected in series with the right circular flexure hinges. The upper component and bottom component are connected in parallel with the end-effector beam. The working principle is shown in **Figure 2(b)**. The elliptical locus will be obtained when two electric sinusoidal signals with phase different are applied to the piezoelectric actuators.

The characteristics of the two types of flexure hinge and deformation schematic of flexure-based mechanism are shown in **Figure 2(c)** and **(d)**, respectively. Sixty-five Mn was adopted as the material of main structural components. In order to investigate the stiffness of the two input displacement directions along the z -axis, the moving direction of the bottom double parallel four-bar linkage mechanism was defined

as the z_1 axis, the upper double parallel four-bar linkage mechanism was defined as the z_2 axis. The stiffness of the guide mechanism in the z_2 axial direction can be considered as a statically indeterminate beam. Then the analytical stiffness modeling was carried out. Meanwhile, a constant force of 1 N was imposed on the input end. Simulation result is shown in **Figure 2(e)**. Additionally, the dynamics analysis was also conducted based on the Lagrange equation and FEA method. It can be seen that if the fixed condition was improved, the second natural frequency will become the first natural frequency, which is helpful to achieve a large working bandwidth. The results of stiffness and natural frequency along the working direction both from analytical modeling and FEA were obtained. The comparison results of FEA and analytical modeling are shown in **Table 1**.

According to the analysis above, a prototype was fabricated. Offline tests were carried out to evaluate the performances. The experimental setup is shown in **Figure 3(a)**. As shown in **Figure 3(b)** are the results of the step responses along z_1 axis and z_2 axis. The rising time are 1.9 ms and 1.5 ms, and the setting time are respectively 3.43 ms and 3.64 ms. There are no steady errors. The amplitude-frequency responses are shown in **Figure 3(c)**. It can be seen that the first natural frequency is about 1200 Hz. The motion stroke and resolution tests are respectively shown in **Figure 3(d)** and **(e)**, the maximum motion stroke of z_1 axis is about 15 μm , the maximum motion stroke of z_2 axis is about 19 μm . The resolution of z_1 and z_2 axes are approximately 15 nm and 30 nm. **Figure 3(f)** shows the real experimental tooltip displacement in different phase shifts, which has a good agreement with the simulation results shown in **Figure 3(g)**. Additionally, the developed EVC vibrator has a good tracking performance and very low crosstalk between the motion axes. However, this vibrator can only be used in orthogonal EVC. The mechanical structure needs further optimization to obtain better performance.

3.1.1.2 Improved type

An improved EVC vibrator was developed aiming to solve the problems discussed above. The mechanical structure of compliant mechanism and the prototype are shown in **Figure 4(a)** and **(b)**. This vibrator not only can be used in orthogonal EVC but also can be used in oblique EVC through angle adjustment of the torque gauge [9]. In order to obtain the best performance, three structure parameters were needed to be further optimized considering the compact structure, high motion stroke and working bandwidth.

The optimization problem was stated first. Objective: $\Delta L(t_1, t_2, r) \geq 30 \mu\text{m}$, $f(t_1, t_2, r) > 3000 \text{ Hz}$. Constraints: $\Delta L_c / \Delta L < 5\%$, $\sigma_{\max} < \sigma_s / n$. Within ranges: $t_1 \in [0.5, 1.5]$ mm, $t_2 \in [0.8, 2.4]$ mm, $r \in [0.5, 1.5]$ mm. In this work, the cutting force was taken into consideration during the structure optimization. A response surface methodology was adopted to establish the relationship between the input variables and output parameters.

	Stiffness (N μm^{-1})		Natural Frequency (Hz)	
	z_1 axis	z_2 axis	3rd	4th
FEA	17.66	16.64	3613.1	4455.1
Analytical model	16.1	16.1	4640.3	4784.7
Deviation (%)	8.8%	3.2%	28.4%	7.4%

Table 1.
 Comparisons results of analytical modeling and FEA method.

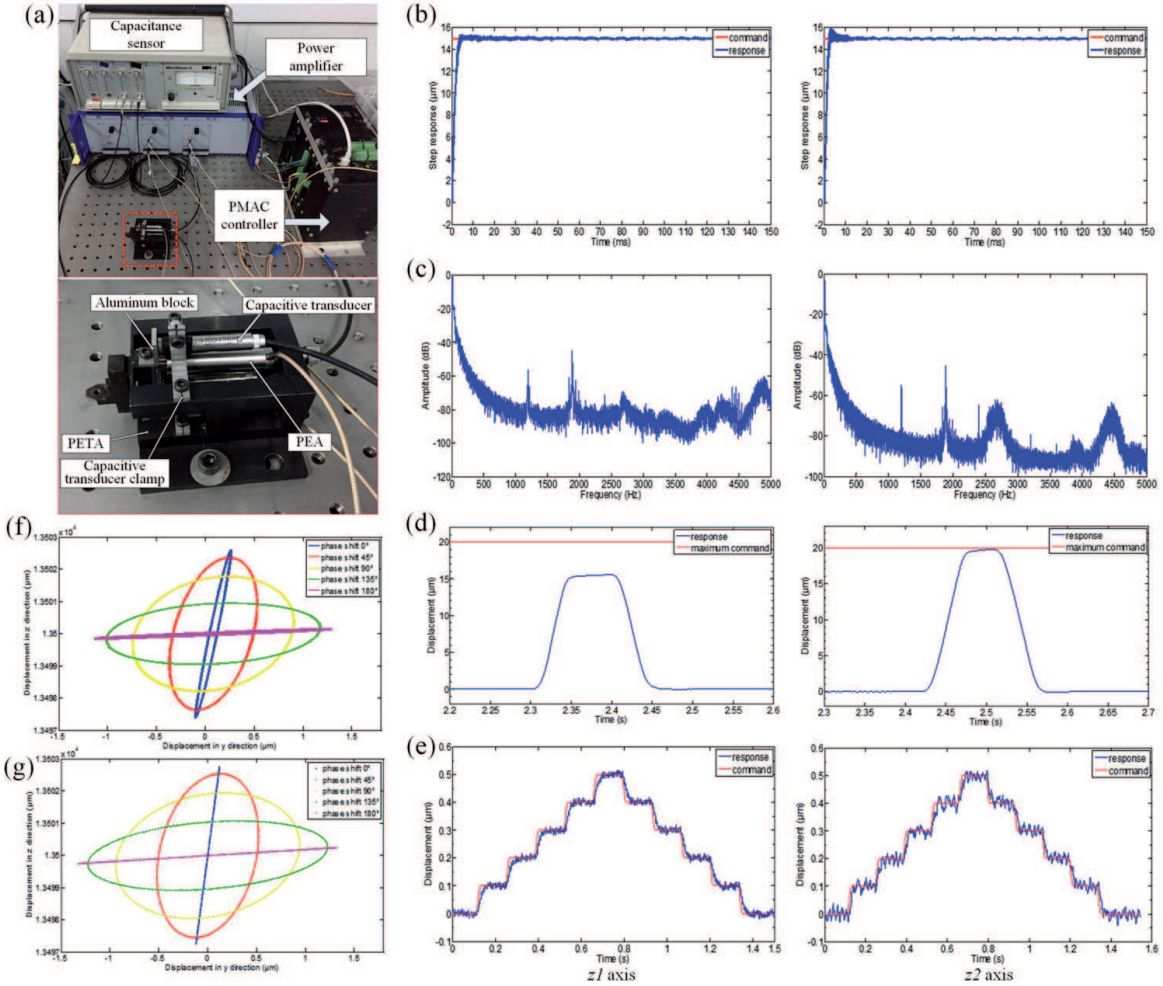


Figure 3. Experimental setup and testing results. (a) Experimental setup. (b) Step responses. (c) Amplitude-frequency responses. (d) Motion stroke. (e) Resolution tests. (f) Experimental results of output tool tip locus with phase shifts. (g) Simulation results of output tool tip locus with phase shifts [8].

An NSGA-II algorithm was used to perform the optimization process. The main process of the optimization can be concluded as follows:

Step 1: Mechanical design is finished first, static and modal analyses are conducted to obtain the response value for the initial design parameters.

Step 2: A response surfaces methodology is adopted to create a predictive model for the design points and the response values. Then, the predicted error should be checked, the other design of experiments methodology or increased experimental design points should be considered when the error is larger than the requirements.

Step 3: MOGA is adopted to deal with the optimization processes via selection, crossover, and mutation. The optimization is converged when the maximum allowable Pareto percentage is realized.

According to the optimization results, a prototype was fabricated with the 7075 T6 aluminum. Offline tests were carried out to evaluate the performance of the optimization vibrator. The results of the step responses along $z1$ axis and $z2$ axis are shown in **Figure 5(a)**. The rising times are 4.4 ms and 4.2 ms. The setting times are respectively 6.7 ms and 9.06 ms. There are no steady errors and overshoots. The amplitude-frequency responses are shown in **Figure 5(b)**. It can be seen that the first natural frequency is about 1800 Hz. The motion stroke and resolution tests are respectively shown in **Figure 5(c)** and **(d)** by using stair excitation signal to each axis, the maximum motion stroke of $z1$ axis is about

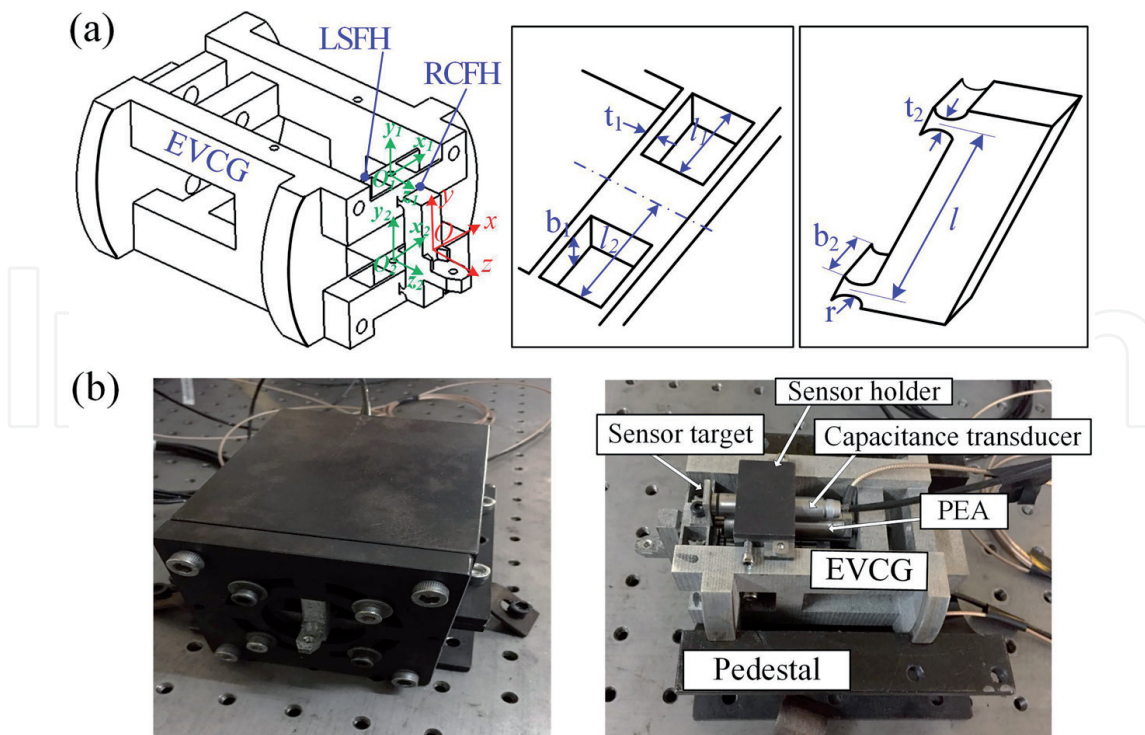


Figure 4. Illustration of the improved EVC device. (a) The compliant mechanism. (b) The prototype [9].

37 μm , the maximum motion stroke of z_2 axis is about 31 μm . The resolution of the z_1 axis and z_2 axis are approximately 9 nm and 10 nm. **Figure 5(e)** shows the motion tracking performance for z_1 axis and parasitic motion for z_2 axis. It can be seen that the maximum tracking error along z_1 axis is 0.7 μm , which is 2.9% of the maximum input displacement. As shown in **Figure 5(f)**, the maximum parasitic motion of z_2 axis is 0.05 μm , which is 0.21% of the maximum input displacement of z_1 axis. For z_2 axis, the maximum tracking error is 0.72 μm , which is 3% of the maximum input displacement. The maximum parasitic motion of z_1 axis is within 0.035 μm , which is about 0.15% of the maximum input displacement. **Figure 5(g)** shows the input signal, the tool vibration locus in 3D space and the projection in xy plane. Compared with the former one, this vibrator has higher modulation ability and commonality for lathes with different configurations.

3.1.2 A flexure-based EVC vibrator actuated by vertical piezoelectric actuator configuration

3.1.2.1 Piezoelectric actuators serial drive

In this work, a flexure-based EVC vibrator with vertical piezoelectric actuator configuration was proposed. In order to avoid the installation error, the base part and the hinge part were designed to be an integral flexure hinge structure [10]. Additionally, the integral flexure part was made from 65 Mn steel. As shown in **Figure 6(a)**, the compliant mechanism was driven by two vertical piezoelectric actuators in serial drive mode. The advantage of this serial design is that the crosstalk between two motion axes can be ignored theoretically. However, the working bandwidth decreases with the increased moving inertia.

The testing experiments were carried out to evaluate the performance. As shown in **Figure 6(b)**, the first natural frequencies along Z direction and Y direction are

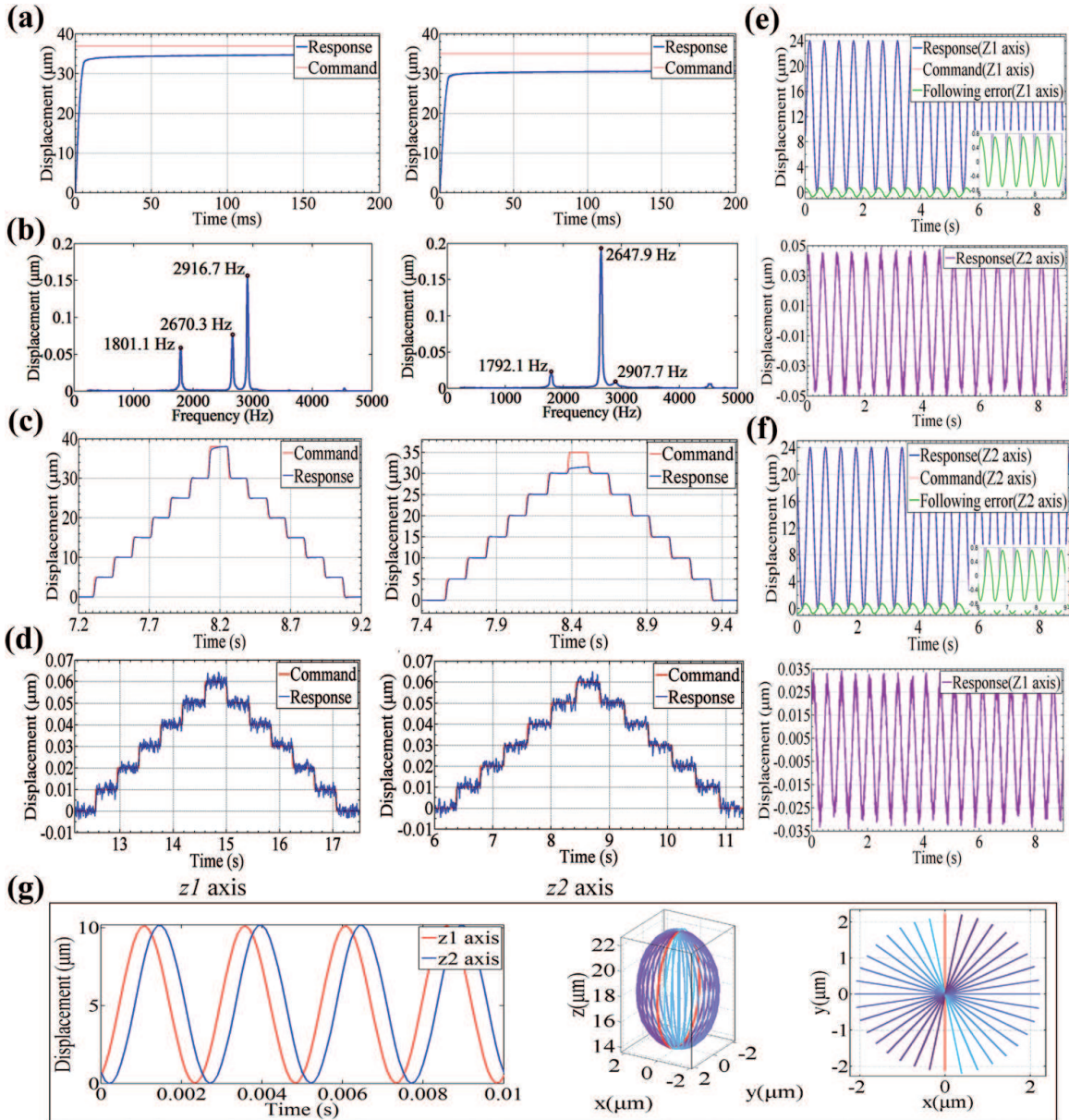


Figure 5. Offline testing results. (a) Step responses. (b) Amplitude-frequency responses. (c) Motion stroke. (d) Resolution tests. (e) Motion tracking for z_1 axis and parasitic motion for z_2 axis. (f) Motion tracking for z_2 axis and parasitic motion for z_1 axis. (g) Input signals and tool vibration locus [9].

1257.74 Hz and 1896.19 Hz, respectively. It can be found from **Figure 6(c)** that the resolution in Z direction and Y direction are all within 8 nm. **Figure 6(d)** and **(e)** show the tracking accuracy and coupling motion in Z direction and Y direction. The maximum following error in Z direction is $0.6 \mu\text{m}$, which is about 1.5% of the full testing stroke. The coupling motion in Y direction is $0.06 \mu\text{m}$, which is 0.6% of the Y-direction testing stroke. The maximum following error in Y direction is less than $0.2 \mu\text{m}$, which is 2% of the testing stroke. The coupling motion in Z-direction can be considered as noise and ignored. **Figure 6(f)** shows the resultant ellipses with different phase shifts and frequencies. It should be noted that the errors in the two directions ascend with the frequency rising. The error in Z-direction is smaller than that in Y-direction. **Figure 6(g)** shows the resultant tool paths with different phase shifts under-cutting speed of $150 \mu\text{m/s}$. **Figure 6(h)** shows the resultant tool paths

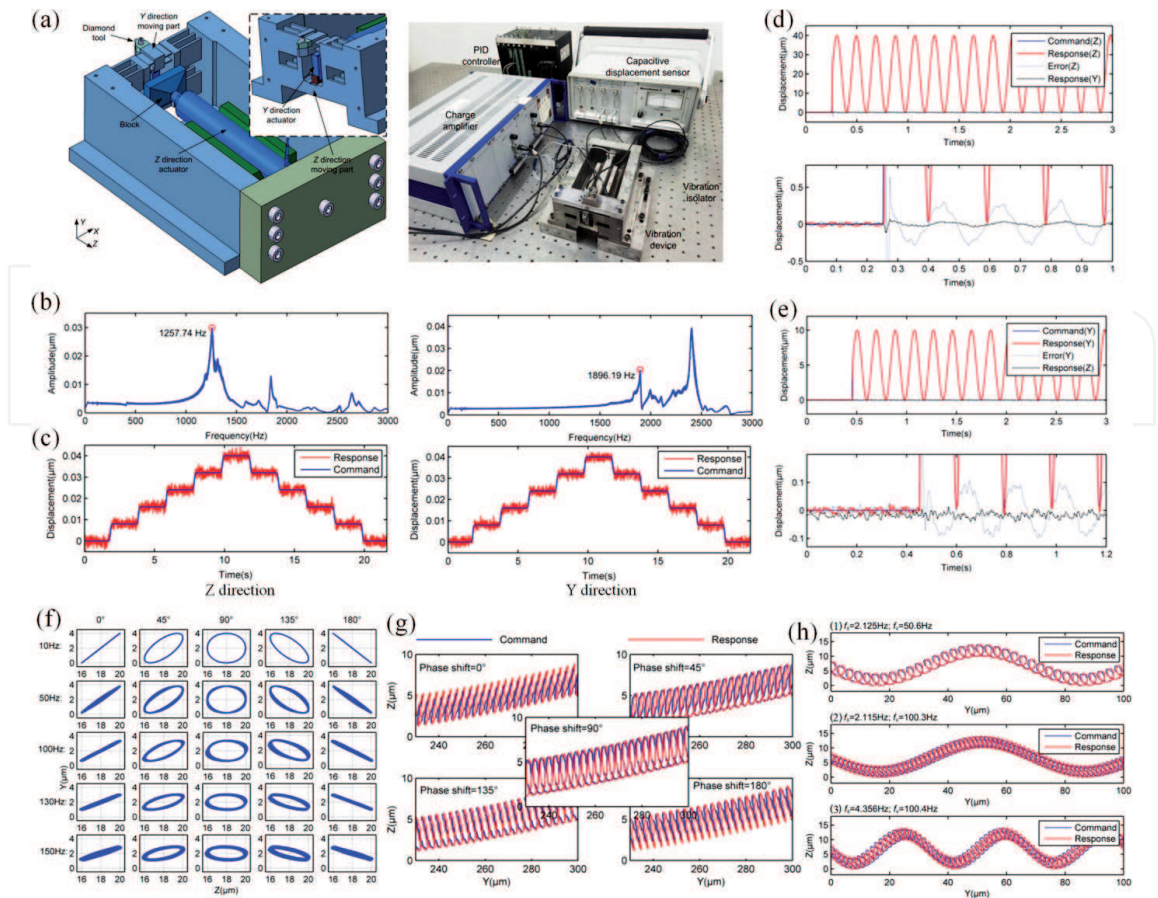


Figure 6. Illustration of mechanical structure, experimental setup and testing results. (a) Mechanical structure and experimental setup. (b) Amplitude-frequency responses. (c) Resolution tests. (d) Motion tracking for Z-axis and parasitic motion for Y-axis. (e) Motion tracking for Y-axis and parasitic motion for Z-axis. (f) Resultant ellipses with different phase shifts and frequencies. (g) Resultant tool paths with different phase shifts. (h) Resultant tool paths at different frequencies [10].

with different frequencies under cutting speed of $150 \mu\text{m/s}$ and 90° phase shift. These two figures demonstrate the double-frequency EVC tracking ability.

3.1.2.2 Piezoelectric actuators parallel drive

Compared with the piezoelectric actuators' serial drive configuration, the parallel drive configuration of piezoelectric actuators is more easy to obtain a higher working bandwidth. However, the cross-axis coupling is a problem that need to be solved.

In general, the mechanical structure decoupling design is usually adopted. In this work, a modified bridge-type amplification mechanism was utilized to meet the requirements among the stroke, output stiffness, resonant frequency, and the drive current [11]. Spring steel was adopted as the material. As shown in **Figure 7(a)**, two perpendicular leaf-spring flexure hinges were applied to decouple the 2D motion. **Figure 7(b)** shows the FEA results of modal analysis. The natural frequency is 6452 Hz and the corresponding mode of vibration is in cutting direction. The mode of vibration in thrust direction corresponds to the natural frequency of 7432 Hz .

In order to evaluate the performance of the prototype. The experimental test was conducted and the experimental setup is shown in **Figure 7(c)**. The sweep experiments were conducted by setting the input voltage amplitudes to 5 V and

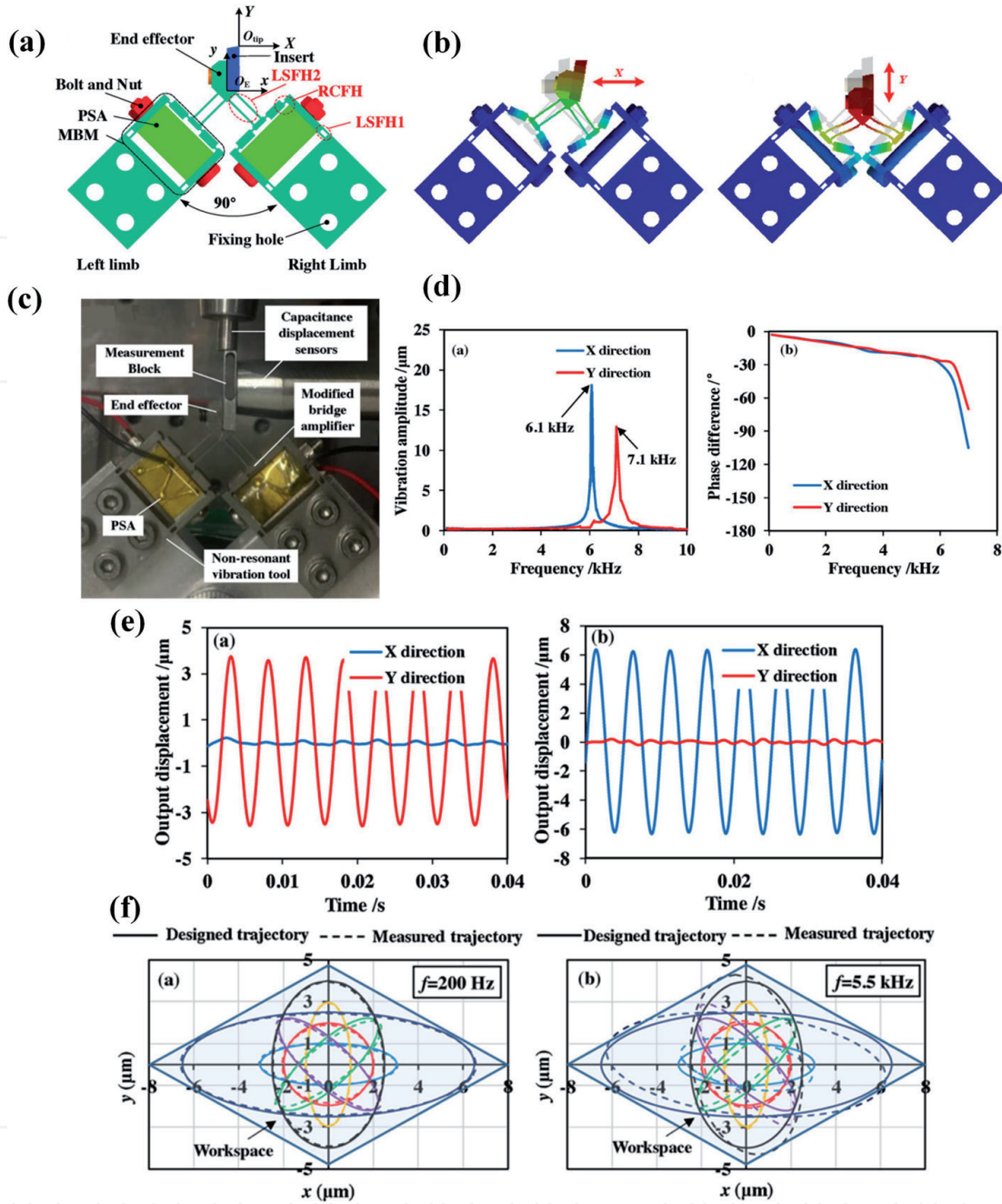


Figure 7. Illustration of mechanical structure, experimental setup, and testing results. (a) Mechanical structure. (b) Modal analysis results. (c) Experimental setup. (d) Frequency response. (e) axis coupling results. (f) Comparison between designed and measured cutting tool locus [11].

the frequency from 0 to 10 kHz linearly. The amplitude-frequency responses and phase-frequency responses are shown in **Figure 7(d)**. The natural frequencies in X and Y directions (i.e. cutting direction and thrust direction) are 6100 Hz and 7100 Hz, respectively, which have good agreement with the results of FEA simulation. Coupling tests of the two motion axes were performed by using sinusoidal signals with frequency of 200 Hz and amplitude of 120 V. The results are shown in **Figure 7(e)** that the coupling ratios between two motion axes are within 5%. The comparison between designed and measured cutting tool locus are shown in **Figure 7(f)** for both low-frequency (200 Hz) and high-frequency (5.5 kHz). The measured results indicate that the agreement between designed and measured ones are good for low frequency.

However, there is a discrepancy between designed and measured ones under higher frequency caused by linearly increasing phase shift which can be eliminated by frequency compensation.

In fact, the angle between two decoupling flexure hinges can influence the decouple performance. A new type of 2 degrees of freedom piezo-actuated pseudo-decouple compliant mechanism was developed which considering the influence of the decoupling angle [12]. As shown in **Figures 8(a)** and **8(c)**, the two perpendicular piezoelectric actuators are configured in parallel. In this work, the influence of decoupling angle Θ on tracking accuracy of elliptical locus was studied by static FEA method. First, a dimensionless aspect ratio λ of the major semi-axis a to the minor semi-axis b of the ellipse locus was introduced. The influence of decoupling angle on the elliptical parameters and relative ratio is shown in **Figure 8(b)**. It can be seen that the developed 2D pseudo-decouple compliant mechanism generated an approximately perfect ellipse locus when the decoupling angle was set to be 102.5° . Then a 3D model of EVC vibrator was established as shown in **Figure 8(c)**. The prototype was manufactured and the experimental tests were carried out to evaluate the performance. Experimental setup is shown in **Figure 8(d)**. **Figure 8(e)** shows the experimental results of kinematic performance. From the resultant tool locus, it can

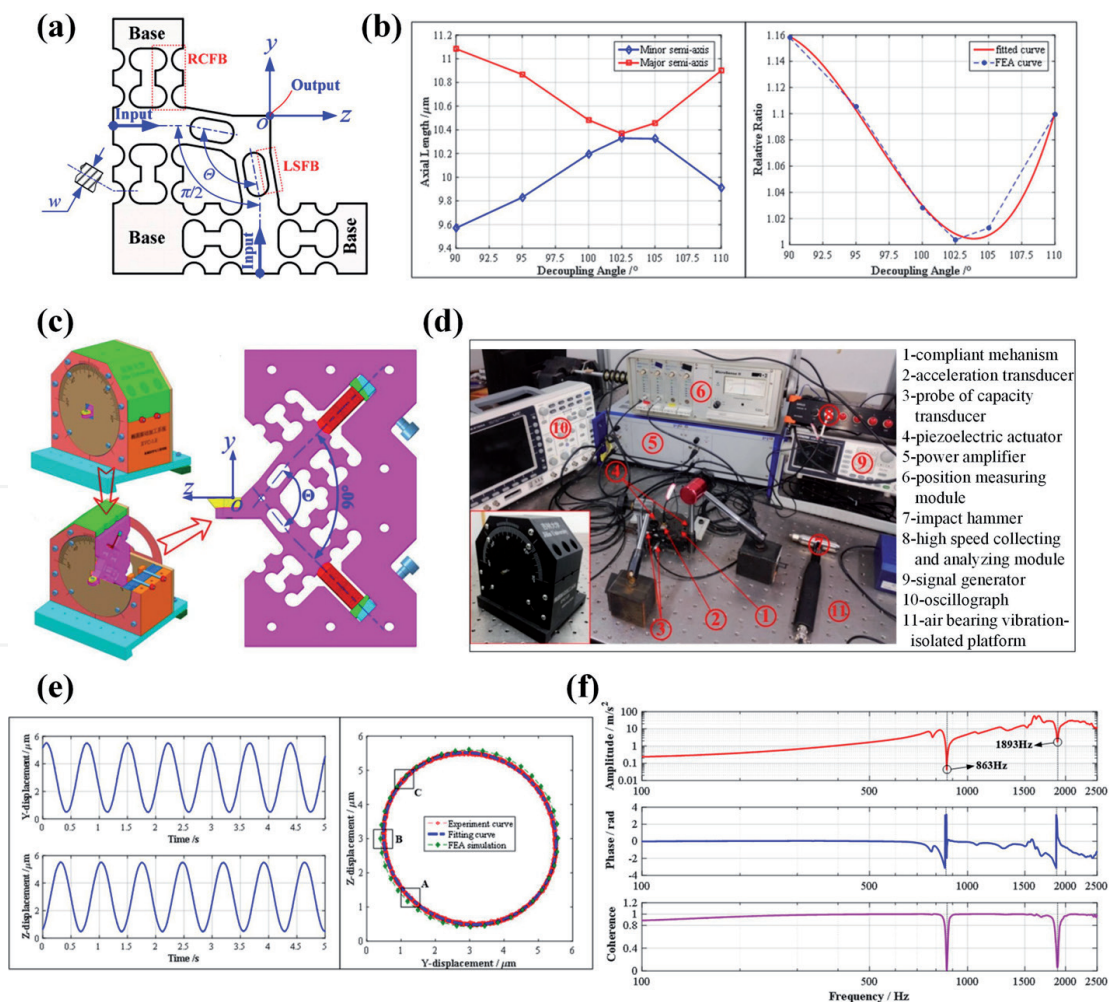


Figure 8. Illustration of mechanical structure, experimental setup, and testing results. (a) Mechanical structure of compliant mechanism. (b) Influence of decoupling angle on the elliptical parameters and relative ratio. (c) 3D model of the EVC vibrator. (d) Experimental setup. (e) Experimental results of kinematic performance. (f) Experimental results of dynamic performance [12].

be seen that the experimental results have a good agreement with the fitted curve and FEA results. **Figure 8(f)** shows the results of dynamic performance by using hammering method. The first two natural frequencies of the pseudo-decouple compliant mechanism are 863 Hz and 1893 Hz, respectively.

3.2 3D type EVC vibrator

3D type EVC vibrator has more degrees of freedom compared with 2D type EVC vibrator. Thus, it has more flexibility and modulation ability to fabricate the structured surface than 2D type EVC vibrator. However, the structure was more complicated and it is difficult to control the structure size, which may influence the potential applications. In recent 10 years, the flexure-based 3D type EVC vibrator developed rapidly. In general, there are three commonly used piezoelectric actuator configurations, i.e. three perpendicular piezoelectric actuators configuration, two parallel and one perpendicular piezoelectric actuators configuration, and four parallel piezoelectric actuators configuration. Here are some typical examples following below.

3.2.1 A flexure-based EVC vibrator actuated by three perpendicular piezoelectric actuators

For 3D type EVC vibrator, three perpendicular piezoelectric actuators configuration are the most commonly used method. A piezoelectric actuated monolithic compliant spatial vibrator with decoupled translational vibration was developed to construct the rotary spatial vibration-assisted diamond cutting system [13]. The 3D model of the rotary spatial vibration-assisted diamond cutting system and the mechanical structure of compliant spatial vibrator are respectively shown in **Figures 9(a)** and **9(b)**. The rotary spatial vibration-assisted diamond cutting system consists of a tool holder, compliant spatial vibrator, piezoelectric actuator, compliant spatial vibrator holder, connection shaft, and fixture. The fixture is used for attaching the whole mechanism onto the spindle of the machine tool through a vacuum chuck. The compliant spatial vibrator and its holder are made of aluminum alloy to reduce the mass of the whole mechanism. The steel was adopted for connecting shaft manufacturing to increase connection stiffness. In this work, a complete compliance modeling was established based on the matrix-based compliance modeling method for compliant spatial vibrator. The dynamic model was established based on Lagrangian principle. FEA simulation was also used to study the static and dynamic characteristics. To evaluate the stroke and parasitic motions, a maximum sinusoid driving voltage ($u = [50 + 50\sin(2\pi t)]$ V) was separately applied to each piezoelectric actuator. The displacement results of compliant spatial vibrator in driving direction and the parasitic motion in other motion directions are shown in **Figure 9(c)**. It can be seen that the practical stroke can reach 11.067 μm , 10.100 μm , and 12.254 μm along the x , y , and z axes directions, respectively. The parasitic motions along y and z axes directions are about $\pm 1.39\%$ and 1.34% with respect to the motion along x -axis direction, respectively. Similarly, the parasitic motions along the x and z axes directions are about $\pm 1.11\%$ and 0.46% with respect to the motion along y -axis direction, respectively. The parasitic motions along the x and y axes directions are about $\pm 1.21\%$ and 0.31% with respect to the motion along z -axis direction, respectively. In addition, the dynamic performance tests were carried out by swept excitation method. Signals with an amplitude of 1.5 V with varying frequency were applied to each piezoelectric actuator, separately. The results of

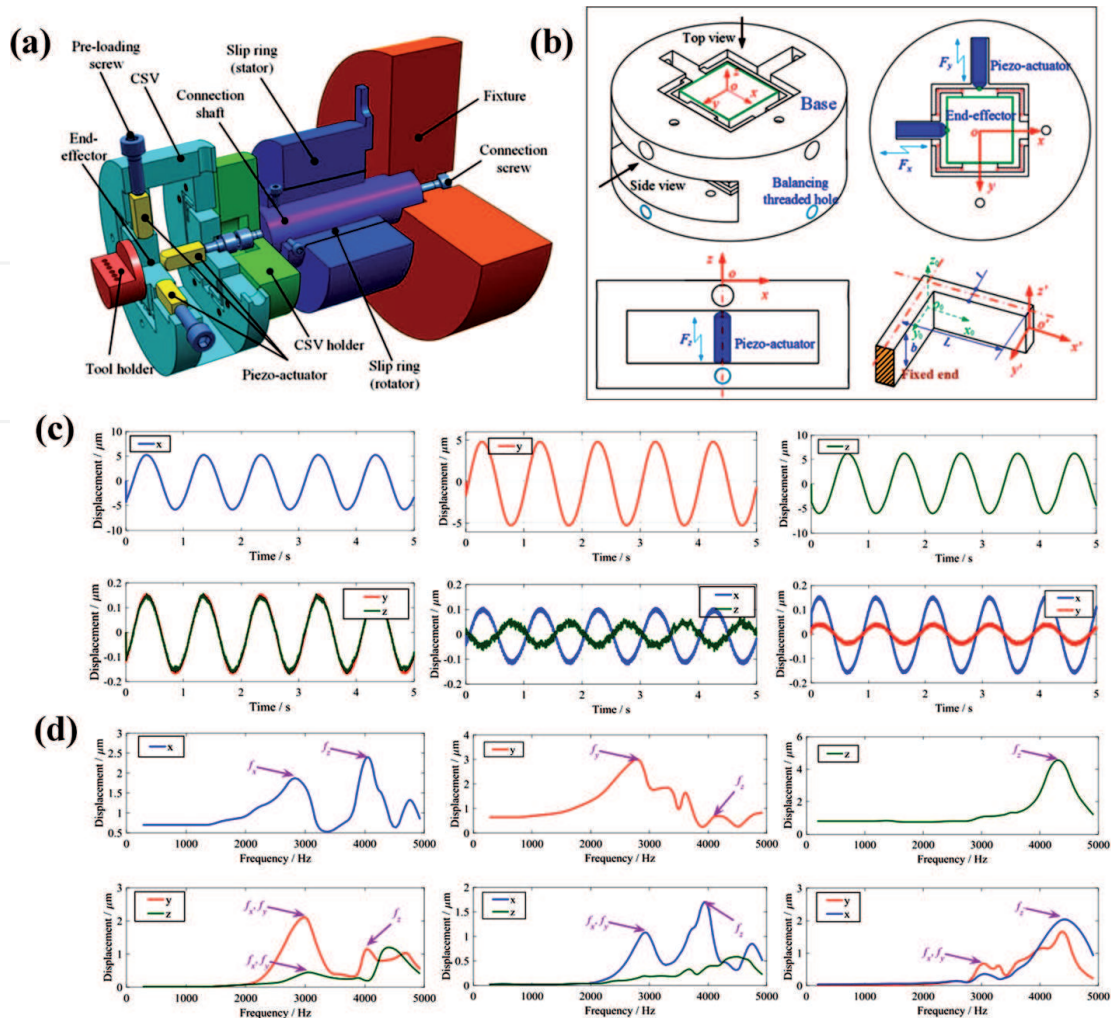


Figure 9. Illustration of 3D model, mechanical structure and testing results. (a) 3D model of the rotary spatial vibration-assisted diamond cutting system. (b) Mechanical structure of the compliant spatial vibrator. (c) Displacement results of compliant spatial vibrator in driving direction and the parasitic motion in other motion directions. (d) Experimental results of dynamic performance [13].

dynamic performance are shown in **Figure 9(d)**. The first natural frequency along x and y axes directions are approximately the same, which are about $f_x = f_y = 2.8$ kHz. While the natural frequency along the z -axis direction is about 4.3 kHz. This vibrator provides a new method for rotary vibration machining.

Different from the above 3D type EVC vibrator, a piezo-actuated tri-axial compliant mechanism was developed to modulate the workpiece for nano cutting [14]. The 3D model of the compliant mechanism is shown in **Figure 10(a)**. Three identical compliant chains were adopted to construct the vibrator. For one compliant chain, the double parallelogram mechanism with eight right circular flexure hinges and a spatial transition mechanism with four sets of parallelogram limbs were adopted. Each limb has two bi-axial right circular flexure hinges. In this work, multi-objective optimal design of the tri-axial compliant mechanism was carried out based on the stiffness modeling, kinematic modeling and dynamic modeling. A Pareto-based multi-objective differential evolution algorithm was utilized to find the global optimal solution.

Then a prototype was manufactured and the performance tests were conducted through the experimental setup which is shown in **Figure 10(b)**. A harmonic signal with frequency of 1 Hz and amplitude voltage of 5 V was applied to each actuator

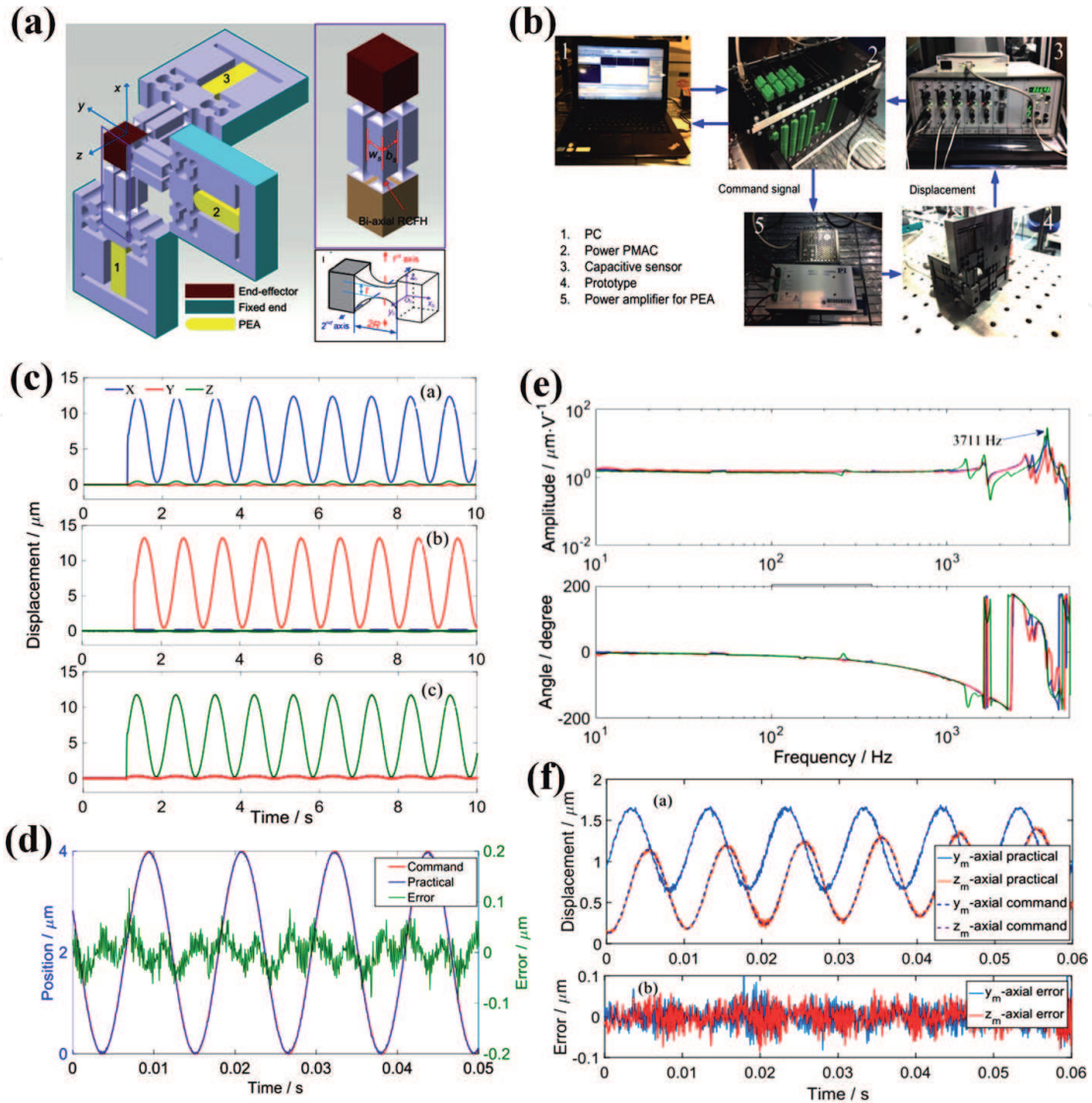


Figure 10.

Illustration of 3D model, experimental setup and testing results. (a) 3D model of the compliant mechanism. (b) Testing experimental setup. (c) Results of harmonic response and the corresponding parasitic motions. (d) Harmonic tracking performance for x -axis. (e) Results of the frequency responses. (f) Harmonic tracking performance for y and z axes during cutting [14].

to assess the motion stroke and the parasitic motion. The results are shown in **Figure 10(c)**, the strokes along x , y and z axial directions are respectively $12.37 \mu\text{m}$, $13.14 \mu\text{m}$ and $11.72 \mu\text{m}$. The maximum parasitic motion (about 3.8%) was generated along z axial direction when driving the piezoelectric actuator along x axial direction. When actuated the piezoelectric actuators along with y and z axial directions, the parasitic motion along the other two directions are almost the same, which are about 1.37% and 2.51% of the corresponding actuation motions. In addition, a typical proportion-integration-differentiation controller is employed for the feedback control. The influences of system noises were eliminated by a low pass filter, and a velocity feedforward compensator was utilized to enhance the response speed. In order to assess the tracking performance, a harmonic signal with frequency of 90 Hz and amplitude of $2 \mu\text{m}$ was adopted as the desired motion. Only the tracking performance along x axial direction was performed to avoid repetition. The tracking results in **Figure 10(d)** shows a tracking error of around $\pm 70 \text{ nm}$, which is about $\pm 1.75\%$ of the motion span. **Figure 10(e)** shows the dynamic performances. The

natural frequency for each direction is around 3.7 kHz due to the identical chain. What's more, the tracking performance along y and z axial directions were also tested during cutting, results of which are shown in **Figure 10(f)**. It should be noted that the noise during cutting is slightly larger than that in offline testing.

3.2.2 A flexure-based EVC vibrator actuated by two parallel and one perpendicular piezoelectric actuators

In this work, a flexure-based EVC vibrator actuated by two parallel and one perpendicular piezoelectric actuator was proposed [15]. The 3D model of the developed

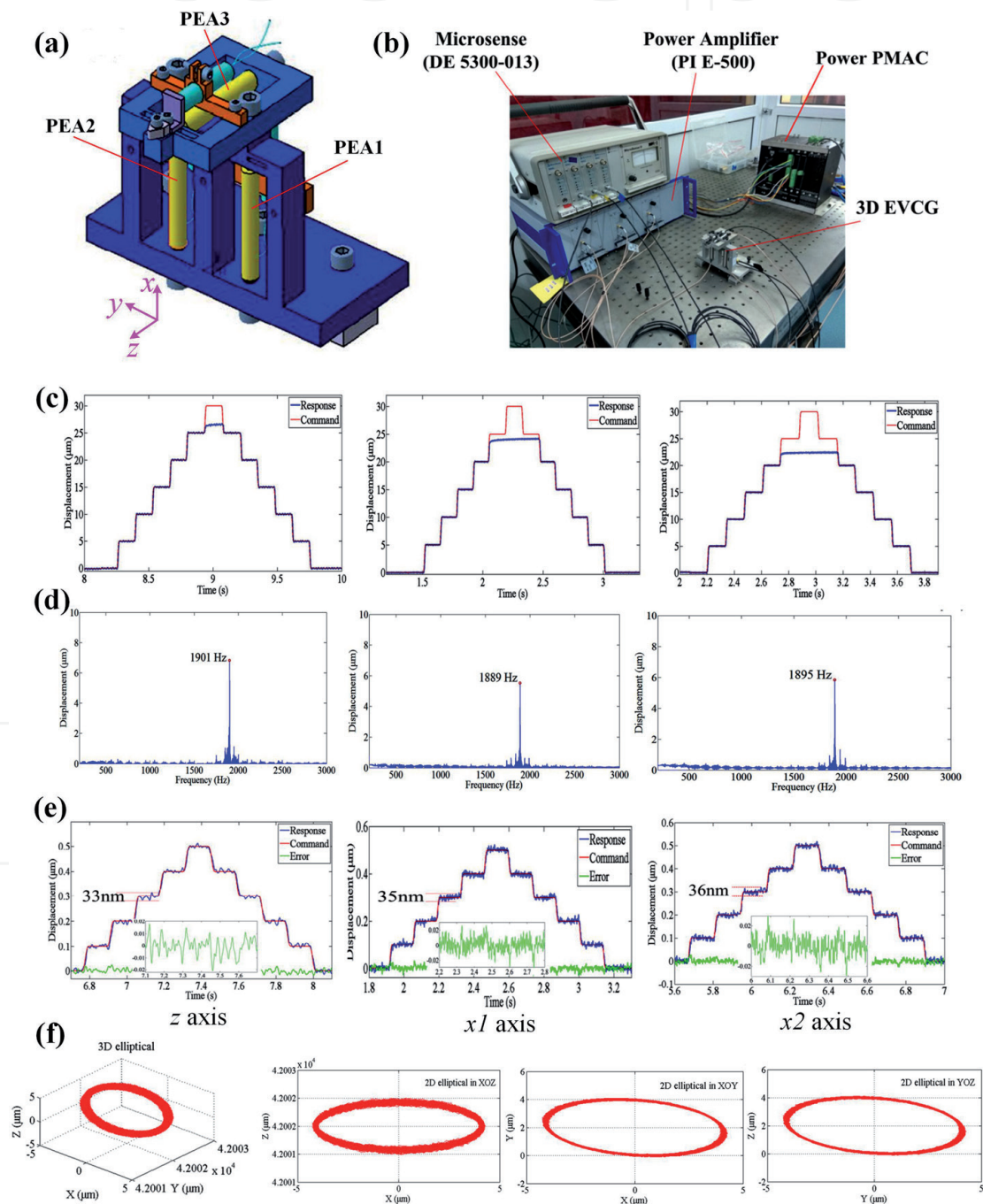


Figure 11. Illustration of 3D model, experimental setup and testing results. (a) 3D model of the developed EVC vibrator. (b) Testing experimental setup. (c) Results of motion stroke. (d) Results of the frequency responses. (e) Results of the resolution test. (f) the synthesized cutting tool locus and the projections [15].

EVC vibrator is shown in **Figure 11(a)**. The EVC vibrator mainly consists of three PEAs (piezoelectric actuators) and capacity probes, two compliant mechanisms. Two compliant mechanisms were independently manufactured considering the complexity of machining. Then the compliant mechanisms were assembled by screws connection. For easy analysis, three axes were defined as follows: axis along PEA1 motion direction was defined as $x1$, axis along PEA2 motion direction was defined as $x2$,

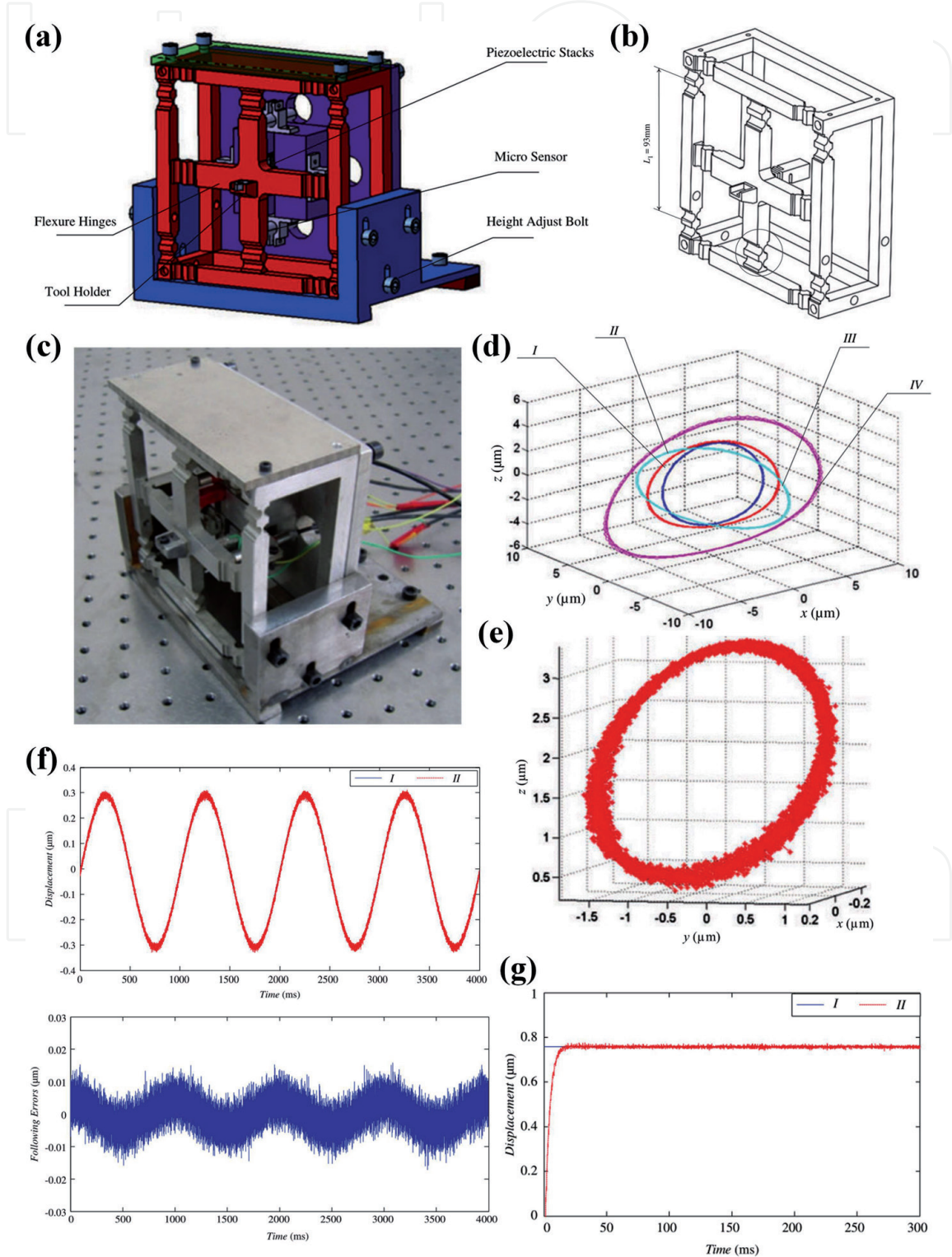


Figure 12. Illustration of 3D model, prototype and testing results. (a) 3D model of the developed EVC vibrator. (b) Mechanical structure of compliant mechanism. (c) Fabricated prototype. (d) Simulated tool locus. (e) Actual tool locus. (f) Tracking performance. (g) Step response [16].

and axis along PEA3 motion direction was defined as z . Additionally, the kinematic modeling was established. The offline tests were carried out to investigate the performance based on the experimental setup shown in **Figure 11(b)**. The motion stroke performances along three axes are shown in **Figure 11(c)**. It can be seen that the maximum displacement along z -axis can reach up to $26\ \mu\text{m}$. The maximum displacements along x_1 and x_2 axes are not the same which are $22\ \mu\text{m}$ and $24\ \mu\text{m}$, respectively, due to the manufacturing error. A swept excitation method with frequency from 100 Hz to 3000 Hz was performed to assess the dynamic characteristics. **Figure 11(d)** shows that the natural frequency along z , x_1 and x_2 axes are about 1901 Hz, 1889 Hz and 1895 Hz, respectively, which is enough for ultra-precision machining. The resolution performance results are shown in **Figure 11(e)** through stair excitation tests. The resolution of motion axes along z , x_1 and x_2 axes are about 33 nm, 35 nm and 36 nm, respectively. Meanwhile, the synthesized cutting tool locus and the projections are shown in **Figure 11(f)** which validate the correctness of the kinematic model and feasibility of the developed EVC vibrator.

3.2.3 A flexure-based EVC vibrator actuated by four parallel piezoelectric actuators

In this work, a flexure-based EVC vibrator actuated by four parallel piezoelectric actuators was proposed [16]. The mechanical structure of the developed EVC vibrator is shown in **Figure 12(a)**. It consists of one fixture base, one compliant mechanism, four piezoelectric actuators and capacity sensors. The compliant mechanism is shown in **Figure 12(b)**, which was fabricated by wire EDM. The prototype of developed EVC vibrator was fabricated and assembled as shown in **Figure 12(c)**. In order to investigate the kinematic characteristics, the kinematic model was established and the simulation results are shown in **Figure 12(d)**, of which I represents reference ellipse, II represents ellipse obtained by changing the acting locations of the four piezoelectric actuators, III represents ellipse obtained by changing the phase shifts of actuated signals, IV represents ellipse obtained by changing the amplitudes of actuated signals. **Figure 12(e)** shows the measured tool locus which is an ellipse in 3D space. The measured tool locus are in accordance with the simulated locus shown in **Figure 12(d)**. **Figure 12(f)** shows the tracking performance in x -direction. A sine wave with amplitude of $6\ \mu\text{m}$ and frequency of 1 Hz was adopted as the command signal. The maximum following error is about 12 nm, which is less than 4% of the full span. The result of step response along x -direction is shown in **Figure 12(g)**. There are almost no overshoot and steady errors by utilizing a typical PID controller.

4. Conclusions

The structured surfaces with various micro/nano characteristics may have different advanced functions in various fields. However, the machining of micro/nano structured surfaces is becoming a challenge for traditional cutting methods on the difficult-to-cut materials. This chapter focus on the EVC technique which is a promising way for structured surface machining. The advantages of EVC were described in detail. Meanwhile, the methods for realization of EVC were also introduced in detail. As is known, the flexure-based non-resonant type EVC vibrator has more flexibility and modulation ability compared with the resonant type EVC vibrator and it has been widely concentrated in recent years. Therefore, this chapter mainly reviews the recent developments and achievements on flexure-based EVC vibrators

actuated by piezoelectric actuators. According to the locus characteristics of cutting tool and its position and posture, the EVC was categorized into three different types. And this chapter reviews some typical examples according to the different types of EVC, including the mechanical structure, working principle of piezoelectric actuator, the static modeling, kinematic and dynamic modeling, structure optimization and testing. Although the flexure-based EVC vibrator developed rapidly, there are still some important problems that severely restricted the performance of EVC vibrator, which need to be further investigated in the future, such as the conflict between high working bandwidth and large working stroke, topological optimization of mechanical structures, fatigue life problems under long working hours, and design of high-performance controller.

Acknowledgements

This work was financially supported by the National Natural Science Foundation of China (Grant No. 51905322) and the Postdoctoral Science Foundation of China (Grant No. 2021 T140420).

Conflict of interest

The authors declared no potential conflicts of interest with respect to the research, authorship, and/or publication of this article.

Author details


Jinguo Han^{1*}, Mingming Lu² and Jieqiong Lin²

1 School of mechanical engineering, Shandong University of Technology, Zibo, Shandong, China

2 Key Laboratory of Micro-Nano and Ultra-Precision Manufacturing of Jilin Province, School of Mechatronic Engineering, Changchun University of Technology, Changchun, Jilin, China

*Address all correspondence to: hankeyee@163.com

IntechOpen

© 2022 The Author(s). Licensee IntechOpen. This chapter is distributed under the terms of the Creative Commons Attribution License (<http://creativecommons.org/licenses/by/3.0>), which permits unrestricted use, distribution, and reproduction in any medium, provided the original work is properly cited. 

References

- [1] Zheng L, Chen W, Huo D. Review of vibration devices for vibration-assisted machining. *The International Journal of Advanced Manufacturing Technology*. 2020;**108**:1631-1651. DOI: 10.1007/s00170-020-05483-8
- [2] Zhu Z, To S, Xiao G, et al. Rotary spatial vibration-assisted diamond cutting of brittle materials. *Precision Engineering*. 2016;**44**:211-219. DOI: 10.1016/j.precisioneng.2015.12.007
- [3] Zhang J, Zhang J, Liu C, et al. Machinability of single crystal calcium fluoride by applying elliptical vibration diamond cutting. *Precision Engineering*. 2020;**66**:306-314. DOI: 10.1016/j.precisioneng.2020.06.008
- [4] Zhang J, Han L, Zhang J, et al. Brittle-to-ductile transition in elliptical vibration-assisted diamond cutting of reaction-bonded silicon carbide. *Journal of Manufacturing Processes*. 2019;**45**:670-681. DOI: 10.1016/j.jmapro.2019.08.005
- [5] Shamoto E, Moriwaki T. Study on elliptical vibration cutting. *CIRP Annals*. 1994;**43**(1):35-38. DOI: 10.1016/S0007-8506(07)62158-1
- [6] Cerniway M A. Elliptical diamond milling: kinematics, force and tool wear. Master Thesis. North Carolina State University. 2002
- [7] Negishi N. Elliptical vibration assisted machining with single crystal diamond tools. Master Thesis. North Carolina State University. 2003
- [8] Lin J, Han J, Lu M, et al. Design, analysis and testing of a new piezoelectric tool actuator for elliptical vibration turning. *Smart Materials and Structures*. 2017;**26**(8):085008. DOI: 10.1088/1361-665X/aa71f0
- [9] Han J, Lin J, Li Z, et al. Design and computational optimization of elliptical vibration-assisted cutting system with a novel flexure structure. *IEEE Transactions on Industrial Electronics*. 2018;**66**(2):1151-1161. DOI: 10.1109/TIE.2018.2835425
- [10] Zhou X, Zuo C, Liu Q, et al. Development of a double-frequency elliptical vibration cutting apparatus for freeform surface diamond machining. *The International Journal of Advanced Manufacturing Technology*. 2016;**87**(5):2099-2111. DOI: 10.1007/s00170-016-8596-2
- [11] Wang J, Du H, Gao S, et al. An ultrafast 2-D non-resonant cutting tool for texturing micro-structured surfaces. *Journal of Manufacturing Processes*. 2019;**48**:86-97. DOI: 10.1016/j.jmapro.2019.10.023
- [12] Wang R, Zhou X, Meng G. Development of a new type of 2-DOF piezo-actuated Pseudo-decoupled compliant mechanism for elliptical vibration machining. *Micromachines*. 2019;**10**(2):122. DOI: 10.3390/mi10020122
- [13] Zhu Z, To S, Ehmann KF, et al. Design, analysis, and realization of a novel piezoelectrically actuated rotary spatial vibration system for micro-/nanomachining. *IEEE/ASME Transactions on Mechatronics*. 2017;**22**(3):1227-1237. DOI: 10.1109/TMECH.2017.2682983
- [14] Zhu Z, To S, Zhu WL, et al. Optimum design of a piezo-actuated triaxial compliant mechanism for nanocutting.

IEEE Transactions on Industrial Electronics. 2017;**65**(8):6362-6371.
DOI: 10.1109/TIE.2017.2787592

[15] Lin J, Han J, Lu M, et al. Design and performance testing of a novel three-dimensional elliptical vibration turning device. *Micromachines*. 2017;**8**(10):305.
DOI: 10.3390/mi8100305

[16] Lin J, Lu M, Zhou X. Development of a non-resonant 3D elliptical vibration cutting apparatus for diamond turning. *Experimental Techniques*. 2016;**40**(1):173-183. DOI: 10.1007/s40799-016-0021-0

IntechOpen